REVIEW

View Article Online
View Journal

(S)TEM-EELS as an advanced characterization technique for lithium-ion batteries

Lei Yu,[a] Matthew Li,[b] Jianguo Wen,[a] Khalil Amine[bc] and Jun Lu*[b]

Although the lithium-ion battery (LIB) has acquired commercial success as a sustainable power source, it still suffers from multiple challenges for the future applications. In order to further develop next-generation batteries, the dynamics of structure change, charge transfer, and ion diffusion occurring inside the battery need to be deeply understood by advanced characterization techniques. (Scanning) transmission electron microscopy-electron energy loss spectroscopy ((S)TEM-EELS) is an effective method for the nano-scale detection of structural and chemical information in materials. This review systematically introduces the advantages and fundamentals of (S)TEM-EELS and its unique applications in LIBs.

1. Introduction

Rechargeable LIBs as advanced power sources have exhibited a level of extraordinary competence in the fields of portable electronic devices and novel hybrid/electric vehicles.[1,2] Furthermore, these applications inspire the development of more superior LIBs with higher energy, faster charge/discharge rates, longer cyclic life, and better safety reliability. As the most crucial components in the LIB, optimizing the current electrode materials and exploiting new electrode materials with stable electrochemical performances are also extremely necessary.[3,4] However, all of these goals need an in-depth understanding of the relationship between the structural changes of battery materials and their performances during the electrochemical process, the degradation mechanism during cycling and aging, the thermal decomposition behaviour at increased temperatures by utilizing various characterization methods, and their combinations.[5–8]

In recent years, tremendous efforts have been made to develop advanced characterization techniques, such as X-ray, electron microscopy, Raman spectroscopy and thermogravimetry.[9–13] Among them, X-ray techniques involving X-ray scattering (such as X-ray diffraction, XRD), X-ray spectroscopy (such as X-ray absorption spectroscopy, XAS) and X-ray imaging (such as transmission X-ray microscopy, TXM) are widely applied for the characterization of LIB under *ex situ* or *in situ* conditions, which provide valuable information about the structural evolution, charge transfer and solid electrolyte interphase (SEI) formation inside batteries.[14,15] They have the obvious advantages of high energy resolutions and non-exotic requirements for the sample preparation. However, their spatial resolutions are relatively poor. Although the current spatial resolutions can reach the scale of a few nanometers by using the synchrotron radiation beam focused using a zone plate, it is still difficult to simultaneously probe the fine structural and spectroscopic changes that occur in the battery, which occur at much smaller length scales. Scanning auger electron spectroscopy (AES) was reported to have sufficient spatial resolution for the probe of element distribution, but the triggered charging effects of the sample usually led to more complicated analysis about the chemical shift, especially for the lithium transition metal oxides with low electron conduction frequently used as cathode materials.[16,17] Besides, energy dispersive X-ray spectroscopy (EDS) is also regarded as a powerful tool to detect the components of materials with high spatial resolution.[18] Unfortunately, it does not have the ability to deal with the light elements like lithium (Li), which is particularly important for LIBs.

In contrast, EELS is an analytical technique sensitive to light elements, which is based on the collection of the changes in the kinetic energy of inelastic scattered electrons to investigate the spectrum of excitation in the matter.[19,20] In practice, EELS is usually combined with TEM or STEM, and Scheme 1 presents a detailed schematic diagram of STEM-EELS. In STEM, high-energy electrons (typically 60–300 keV) are used as incident electrons to interrogate the sample. They can be focused into a very small probe size by electromagnetic lenses. Currently, the sub-0.1 nm size is achieved by using an aberration-corrector above the TEM specimen, thereby increasing the spatial resolution to atomic dimensions.[21] The converged electron beam will then pass

[a] *Center for Nanoscale Materials, Argonne National Laboratory, 9700 South, Cass Avenue, Lemont, IL 60439, USA*
[b] *Chemical Sciences and Engineering Division, Argonne National Laboratory, 9700 South, Cass Avenue, Lemont, IL 60439, USA. E-mail: junlu@anl.gov*
[c] *Institute for Research and Medical Consultations (IRMC), Imam Abdulrahman Bin Faisal University (IAU), Dammam 34212, Saudi Arabia*

through the specimen. High-angle annular dark-field (HAADF) images can be captured using an annular detector to collect scattered electrons with high angles. Simultaneously, EELS can also be acquired by using the transmitted beam after passing through a magnetic prism. This is one of the key advantages of EELS performed in (S)TEM, enabling the easy achievement of atomic-level images and spectra at the same time.[22] When the transmitted electrons are collected at a small scattering angle, the transitions of core electrons basically follow the dipole selection rule.[23] At this time, EELS is essentially equal to XAS and is capable of probing the energetics and coordination environments of materials, which is very useful for studying the localized structure and chemical states in the LIB.

By virtue of the aforementioned advantages, (S)TEM-EELS has gradually became a necessary method to account for the microscopic transport of Li^+ ions, oxygen release and charge transfer of transition metal in the current reports.[24–27] However, to our knowledge, there is no systematic review that summarizes the applications of (S)TEM-EELS on LIBs to date. In this paper, we reviewed the basic principle of EELS and its different applications in the field of LIBs. Furthermore, we also put forward reasonable prospects for the future development that should be helpful and bring new insights to other researchers.

2. Fundamentals of EELS

When high-energy electrons impact matter, some of electrons will interact with the constituent atoms by electrostatic forces. This is due to the fact that the incident electrons and the components of an atom (nucleus and atomic electrons) are all charged particles. Under this interaction, these electrons will be scattered (changed in direction) either elastically (no energy exchange) or inelastically. Since the mass of the atomic nucleus is much greater than that of the electron, the energy exchange of interaction between incident electron and nucleus is extremely small and usually unmeasurable. Hence, the incident electron interacting with the nucleus is considered to be elastically scattered. On the other hand,

Lei Yu

Lei Yu is currently a graduate research at the Nanoscience and Technology division in Argonne National Laboratory. His research interest is mainly focused on the fundamental investigation of battery materials using advanced electron microscopy characterization techniques.

Jun Lu

Dr Jun Lu is a chemist at Argonne National Laboratory. His research interests focus on the electrochemical energy storage and conversion technology, with the main focus on beyond Li-ion battery technology. Dr Lu earned his bachelor's degree in Chemistry Physics from the University of Science and Technology of China (USTC) in 2000. He completed his PhD from the Department of Metallurgical Engineering at University of Utah in 2009. Following a DOE-EERE postdoctoral fellow under Vehicles Technology Program, he joined the Division of Chemical Sciences and Engineering at Argonne National Laboratory as a chemist in 2015. He was elected as Associate President and a board committee member of the International Academy of Electrochemical Energy Science (IAOEES). Among his many awards, he is recipient of the R&D 100 Award in 2019; IBA early career research award in 2020; ENFL Emerging Researcher Award from ACS in 2019; IALB Young Investigator Award in 2016; first awardee of IAOEES Award for Research Excellence in Electrochemistry Energy in 2016, the awardee of the first DOE-EERE postdoctoral fellow under Vehicles Technology Program from 2011 to 2013. He also served as the associate editor for ACS Applied Materials and Interfaces since 2016. He was ranked as the Global Highly Cited Researchers (top 1% by citation) by Clarivate Analytics in 2018–2020. He has authored/coauthored more than 420 peer-reviewed research articles, published in Nature, Science, Nature Energy, Nature Nanotechnology, Nature Review Materials, Chemical Reviews, Chemical Society Reviews, Nature Communications, Journal of the American Chemical Society, Advanced Materials, Angewandte Chemie etc., and has filed over 20 patents and patent applications.

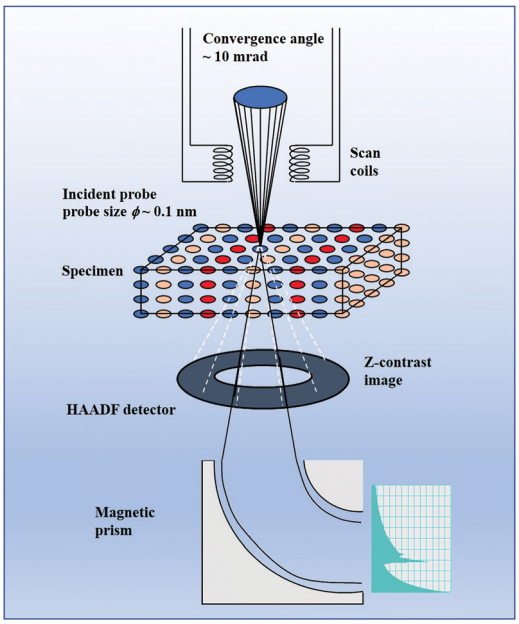

Scheme 1 Schematic diagram of STEM-EELS.

inelastic scattering involves the interaction of incident electrons with atomic electrons, in which the incident electrons lose an appreciable amount of energy to excite the atomic electrons to higher energy levels. Recording the primary process of electron excitation gives rise to the corresponding EELS spectrum.

As shown in Fig. 1a, a typical EELS spectrum is composed of a zero-loss peak (ZLP), low-loss and high-loss regions. ZLP, as its name implies, appears at 0 eV and suggests the transmitted electron without suffering measurable energy loss. It includes all the elastically and quasi-elastically scattered electron (like phonon scattering) components. When the thickness of specimen is less than the plasmon mean free path (MFP), ZLP is the most intense characteristic peak in the EELS spectrum, and the full width half-maximum (FHWM) of ZLP can act as an indicator of spectral energy resolution. The low-loss region usually refers to the energy loss region of 0 to 50 eV, which corresponds to the excitation of electrons in the outermost atomic orbitals within a matter.[28,29] The prominent feature in the low-loss region is a broad peak (called plasmon) located at 3–30 eV, originating from the collective resonant oscillations of valence electrons. In addition to the collective responses, the excitation of single electron also can be observed in the form of fine-structure peaks at the low-loss region, which represents the interband transitions between valence and conduction bands. Upon deeply analysing the low-loss spectrum one can get various pieces of information such as the thickness, dielectric constant, band gap and free-electron density of the sample.

The high-loss region, ranging from 50 eV to several thousand electron volts, corresponds to the excitation of atomic electrons in the inner shell.[30] Owing to a strong binding with the nucleus, the collective effects of these electrons are negligible, and inner-shell excitation mainly refers to the transitions of core electrons to unoccupied states above the Fermi level. Their excitation presents the profile of ionization edges in the spectrum and superimposes on the exponentially decreasing background. The threshold of the ionization edge, corresponding to the core-electron binding energy, is a characteristic value for a particular atom and electron subshell. Based on this, component elements can be distinguished in the specimen. Furthermore, after accounting for the background, edge intensities also allow quantitative analysis of the elements. The intensity fluctuations from 10 to 50 eV after the edge onset represent the EELS near-edge fine structure (ELNES), which alludes to the density of empty electronic states.[31,32] ELNES analysis is usually coupled with Density Functional Theory (DFT) calculations to determine local crystallographic and electronic structures of the excited atom. Beyond the near-edge region, there is also a region of weaker and extended oscillations known as the extended energy-loss fine structure (EXELFS). Similar to extended fine structure of XAS (EXAFS), the signals in this region can be used to analyse the bond length between atoms and their coordination numbers.

Since the LIB materials commonly contain Li, O and transition metal (TM) elements, we focus on the typical Li-K edge, O-K edge and TM-L edge spectra as shown in Fig. 1b–d, respectively.[33–35] From Fig. 1b, various Li-containing compounds show the significantly different fine structures of Li-K edge based on their different atomic environments surrounding Li. Normally, these distinctions can be recorded as fingerprints to identify the chemical composition of materials. In the O-K edge spectra of Fig. 1c, it is clear that the prepeak is sensitive to the valence state of TM. The prepeak of the O-K edge spectra stems from the transition of electrons from the O-1s core level to the unoccupied O-2p states hybridized with TM-3d orbitals, and its intensity directly reflects the extent of

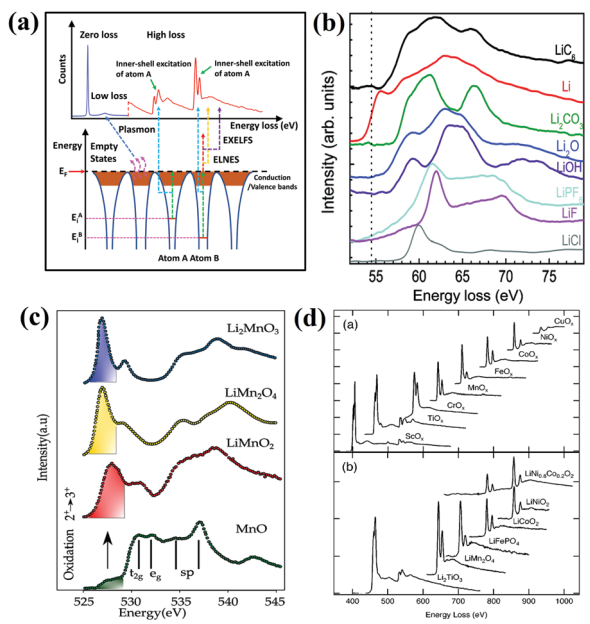

Fig. 1 (a) Schematic illustration of a typical energy-loss spectrum, and three main edges for LIB: (b) Li-K edge, (c) O-K edge and (d) TM-L edges. (b) Reprinted with permission from ref. 33. Copyright 2011, American Chemical Society. (c) Reprinted with permission from ref. 34. Copyright 2020, American Chemical Society. (d) Reprinted with permission from ref. 35. Copyright 2004, American Physical Society.

TM_{3d}–O_{2p} hybridization.[36] In addition, as displayed in Fig. 1d, the TM-L edges are characterized by two white lines of L_3 and L_2, corresponding to the transition of electrons from $2p_{3/2}$ and $2p_{1/2}$ spin–orbit split levels to unoccupied 3d states of TM.[37] The relative energy position and intensity of these two lines strongly rely on the 3d orbital occupancy and hence on the oxidation state of TM elements.[38–40] Comprehensive analysis of these three edges is remarkably helpful to explain various phenomena occurring at the electrochemical process.

Several factors can affect EELS detection and elemental analysis. Multiple inelastic scattering occurs when the thickness of the specimen is greater than the MFP for inelastic scattering (roughly 100 nm at 100 keV). It can significantly enhance the plasmon intensities, leading to an increase in the background contribution, thereby drowning out the signal of ionization edges in a spectrum. Furthermore, the mixed inelastic scattering involving core-level and plasmon excitations will result in a broad peak above the ionization threshold. Currently, the unwanted multiple inelastic scattering contribution can be removed by Fourier transform deconvolution techniques (Fourier-log and Fourier-ratio methods) at the cost of adding some noise. To ensure a sufficient signal/noise ratio, it is best if the thickness of the specimen is close to and lower than the MFP, and the ultrathin specimen should be avoided. On the other hand, in the case of acquiring high spatial resolution STEM-EELS, it is inevitable to introduce beam damage due to the overlapping of scanning probes. Battery materials like layered transition metal oxides are easily converted to spinel or rock-salt structures under an intense electron beam. Therefore, a good balance between the probe current, spatial resolution and the acquired signal/noise ratio should be made to avoid the beam induced artifacts.

3. Applications of EELS for LIB

3.1 Tracking of Li^+ ions migration

With the increasing demands of customers, a fast-charging capability has become an indispensable skill for next-generation LIBs. The fast-charging battery usually requires electrode and electrode active materials to possess high ion diffusion coefficients.[41,42] However, experimental results demonstrated that the lithium titanate ($Li_4Ti_5O_{12}$) anode exhibited poor Li diffusion in both its phases, but still possessed extraordinary rate performances, which conflicts with conventional ideas. To thoroughly clarify the underlying mechanism, Zhang *et al.* designed a novel TEM grid-based electrochemical cell for the operando Li-EELS measurements with high spatial and temporal resolution.[43] The corresponding results are shown in Fig. 2a. During discharging–charging, it is found that the main peak of Li-EELS remains almost unchanged at the energy position, whereas the prepeak region presents obviously different fine structures. A new prepeak labeled as "M" appears at the electrochemical process, but it is absent at the charging and discharging products. Furthermore, the Li-EELS tested at different current rate indicated the intensity of prepeak "M" is strongly rate-dependent (Fig. 2b). This presented features in the Li-EELS spectra provide

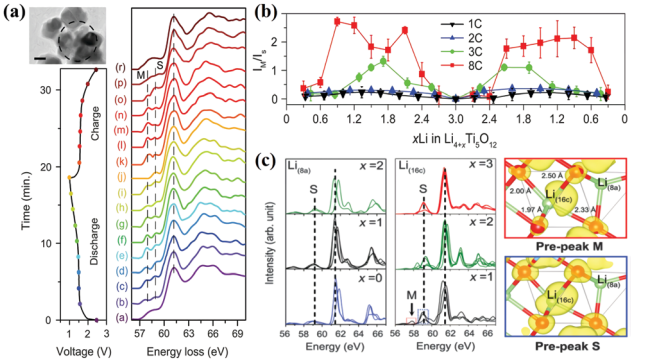

Fig. 2 (a) Voltage profiles of $Li_4Ti_5O_{12}$ nanoparticles and the corresponding EELS spectra selected with an interval of 120 s during the first cycle at 2C rate. (b) Intensity ratio of the two prepeaks, M and S (I_M/I_S) as a function of Li concentration (x) at different rates (1C, 2C, 3C, and 8C). (c) Calculated Li-EELS spectra of $Li_{4+x}Ti_5O_{12}$ (x = 0, 1, and 2) for Li at 8a sites and $Li_{4+x}Ti_5O_{12}$ (x = 1, 2 and 3) for Li at 16c sites, respectively. Adapted with permission from ref. 43. Copyright 2020, The American Association for the Advancement of Science.

the vital information about the occupancy and fast migration of Li^+ in the metastable intermediates ($Li_{4+x}Ti_5O_{12}$) located along the boundary between the two phases. DFT calculations validated that the prepeak of "M" results from the splitting of Li–O anti-bonding states associated with the local distortion of face-sharing Li polyhedra (Fig. 2c).

Hence, a detailed mechanism about the migration of Li^+ in $Li_4Ti_5O_{12}$ during the electrochemical process was presented by the authors. Firstly, the observed high-rate performance stems from the rapid migration of Li^+ at the boundary between the two phases, which involves face-sharing Li polyhedra. At each step of migrating Li^+, the number of face-sharing Li polyhedra in transition state is less than it in the initial and final states. The relatively reduced repulsion between Li^+ in the transition state likely benefits to decline the activation barrier. On the other hand, the local distortion of face-sharing Li polyhedral also can reduce the effective coordination numbers of Li, especially for the electrode at a high rate with more highly distorted Li polyhedra. Hence, when Li^+ ion migrates through the three-coordinated oxygen face, the change in Li coordination is minimized, thereby further reducing the activation barrier. Combining these two aspects of factors, the migration of Li^+ in $Li_4Ti_5O_{12}$ during the electrochemical process exhibits the low migration barrier.

3.2 Monitoring of local charge density around O atoms

Lithium transition metal oxides are the most commonly used electrode materials for LIB, and it is well known that they store charge through the rapid extraction/insertion of Li^+ ions.[44,45] However, about the changes of electronic structures during the extraction/insertion process are still short of full understanding. Conventional chemical ideas assume that Li and O atoms are ionized as Li^+ and O^{2-} ions in the oxides. Hence, the extraction/insertion of Li^+ ions are considered to just influence the charge of TM atoms. This description lacks information on local electronic structure and also neglects the electronic configuration of covalency.

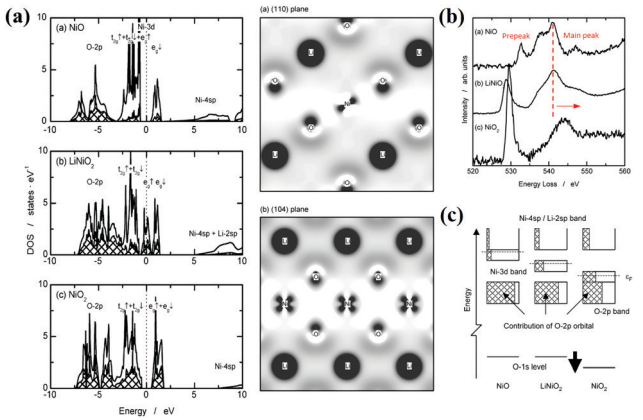

Fig. 3 (a) Density of states calculated for NiO, $LiNiO_2$, and NiO_2 and difference in electron density distribution between $LiNiO_2$ and NiO_2 on (1 1 0) and (1 0 4) planes, (b) O-K edge ELNES, and (c) schematic electronic structures of NiO, $LiNiO_2$, and NiO_2. Adapted with permission from ref. 46. Copyright 2005, American Chemical Society.

In view of this, Koyama and co-workers investigated the detailed electronic structure of NiO, $LiNiO_2$ and NiO_2 by first-principles calculations and EELS.[46] Among them, the NiO_2 was prepared by electrochemical lithium extraction of $LiNiO_2$. The density of states and charge density distribution based on first-principles calculations (Fig. 3a) manifested notable decreases in charge density at nickel and oxygen atoms after lithium extraction from $LiNiO_2$ to NiO_2. This implies that the oxygen atoms also take part in the solid-phase redox reaction of $LiNiO_2$. The experimental EELS results of O-K edges are exhibited in Fig. 3b. As above discussion, normally, the intensity and position of O-K edge prepeak becomes stronger and shifts to lower energy loss with the increase of TM valence, owing to the enhanced TM_{3d}–O_{2p} hybridization and decreased TM-3d energy. However, it is found that the O-K edge energy of NiO_2 is not suitable for this rule. The prepeak of NiO_2 is located at a higher energy than that of $LiNiO_2$. Furthermore, the energy of main peak is also higher than that of NiO and $LiNiO_2$. The whole shift of O-K edge toward higher energy suggests the reduction of electron density at oxygen atoms, in accordance with first-principles calculations. The reason can be explained as follows: the increased oxidation of the nickel atoms strengthens the covalent bonding between the nickel and oxygen atoms with the extraction of Li^+ ions, thereby leading to a relative reduction in electron density around the oxygen atoms. A schematic diagram about electronic structures of NiO, $LiNiO_2$ and NiO_2 was built, as shown in Fig. 3c. The prepeak energy of NiO_2 is affected by the combined energy changes of O-1s level and Ni-3d band.

3.3 Detection of the chemical state of TM atoms

Cyclic stability is an extremely important performance indicator for the practical applications of LIB. Therefore, a large number of research groups conducted extensive investigations on the degradation mechanism involving structural evolution of electrode materials.[47,48] For the layered transition metal oxides, it is well known that the layered structure phase will be gradually transformed into the spinel phase and eventually deteriorate into the rock-salt phase *via* the long-time electrochemical cycles. The phase transition of materials can be accurately identified by high-resolution TEM (HRTEM) and diffraction patterns (Fig. 4a).[49] Along with phase transition, the induced valence changes also can be fully detected by EELS. As shown in Fig. 4b, a line-scan EELS was performed on a cycled electrode particle from bulk to surface, and the corresponding test results are presented in Fig. 4c. The decrease of O-K edge prepeak is an indirect evidence for the reduction of TM valence states. Not only that, both the increased L_3/L_2 ratios and the shifts of L-edge toward lower energy further indicate the decline of TM valence states at the particle surface, which is mainly due to fact that the surface is frequently subjected to the attack of the electrolyte. The precise valence states of corresponding elements can be determined by combining DFT calculations and comparing fine structure with the standard spectra.

However, the materials with same phase structure is difficult to distinguish by HRTEM and diffraction patterns. For example, there are currently three well-known Mn-based spinel phases: $Li_4Mn_5O_{12}$ (Mn^{4+}), $LiMn_2O_4$ ($Mn^{3+/4+}$), and TM_3O_4-type ($Mn^{2+/3+}$). The best way to distinguish them is to utilize their differences in valence. Recently, Zhang *et al.* reported a novel $Li_xTM_{3-x}O_4$-type spinel shell prepared by preliminary electrochemical activation to protect the interior electrode material.[50] The EELS results demonstrated the obviously stable structure in the bulk with the help of

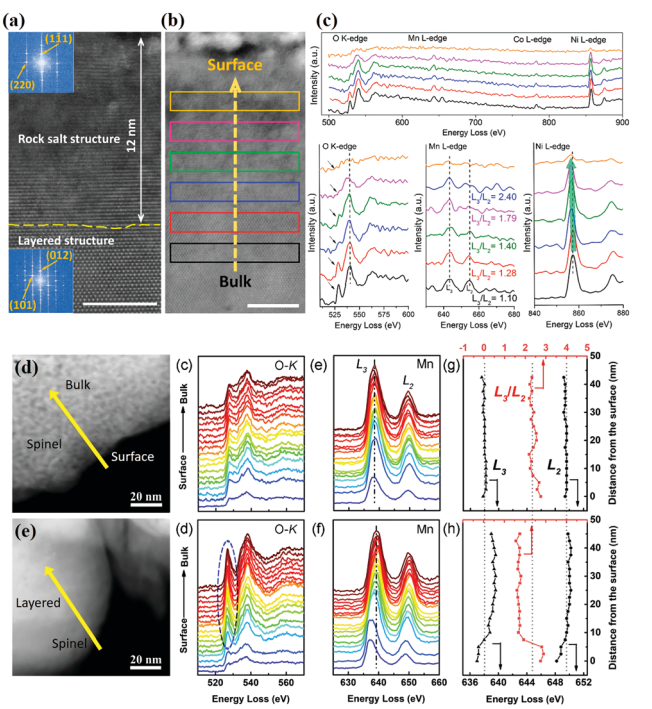

Fig. 4 (a) Atomic-level STEM-HAADF image of a bare NMC811 cathode after cycling with corresponding FFT patterns inset. (b and c) STEM-HAADF image and corresponding EELS spectra acquired from the regions. Reprinted with permission from ref. 49. Copyright 2019, American Chemical Society. HADDF images and corresponding line-scan EELS profiles of the normal Li-rich electrode (d) and the activated Li-rich electrode (e). Reprinted with permission from ref. 50. Copyright 2020, Elsevier.

the preformed spinel shell (Fig. 4e). Furthermore, the preformed spinel shell showed a lower Mn valence than the spinel phase produced by routine electrochemical cycling (Fig. 4d and e). A further detailed analysis about the energy positions and ratios of $L_{3,2}$ indicated that the spinel structure caused by routine electrochemical cycles belongs to $LiMn_2O_4$-type, and the preformed spinel shell belongs to $Li_xTM_{3-x}O_4$-type.

4. Conclusions and outlooks

In this review, the advantages and fundamentals of (S)TEM-EELS as a nanoscale characterization technique were summarized in detail. The high sensitivity for light elements and high spatial resolution make (S)TEM-EELS very suitable for detecting the local structures and chemical states inside LIB. Various phenomena occurring in the battery involving the migration of Li^+ ions, the local electronic structure changes and phase transition were also discussed from three typical EELS ionization edges based on the most common elements in the LIB materials, which are difficult to illustrate by other characterization methods.

In recent years, the EELS technique has gained significant progress with the ever-increasing number of applications. This has been especially true for improvements in spatial and energy resolution with the development of a more advanced aberration-corrector and monochromator, which provides more possibilities in the characterization of LIB.[51–53]

Cation doping has long been regarded as an effective way to improve the performances of layered electrode materials.[54–56] According to their own characteristics, doping atoms can reside in the Li slabs or the TM slabs, resulting in different roles in electrochemical performances. Researchers have typically relied upon theoretical calculations to predict the structure and coordination environments of heteroatoms, whereas atomically resolved EELS can provide a truly local investigation of the chemical state of heteroatoms. Furthermore, during the electrochemical process, a highly active electrode surface is frequently subjected to an attack from the electrolyte, thereby yielding severe structure degradation. To address this issue, the conventional mitigation strategy is to passivate the surface with an inactive coating (such as Al_2O_3 and AlF_3).[57,58] However, there is still no in-depth understanding of the relationship between surface active sites and coatings. Atomically resolved EELS is also expected to reveal their relationship. Apart from these, the minor energetics changes at defects, the incubation of cracks and structure transition in the particle boundary all require more explanations with the help of ultra-high spatial resolution EELS.

On the other hand, a low-loss region is not often used in the analysis of LIB materials. While with greatly improved energy resolution in monochromated EELS, more fine structures can be resolved in low-loss region. It was reported that the fine structures in the interband transition regions of several cathode materials are unique and are sufficient to be used in fingerprint analysis.[59] Another advantage of monochromated EELS is its ability for detecting chemical species without direct electron beam interaction with sample. The signal acquisition of the low-loss region is not as dependent on the sample thickness and electron doses as the high-loss region. This could be used for studying local chemical changes of beam sensitive substances such as the SEI layer and the electrolyte. In addition, a recent publication showed that monochromated EELS enables detection of local phonon changes induced by a stacking default.[60] This capability may also be used to study the evolution of Li in electrode materials, since local phonon changes depend on Li distribution.

Conflicts of interest

There are no conflicts to declare.

Acknowledgements

This work was performed at the Center for Nanoscale Materials, a U.S. Department of Energy Office of Science User Facility, and supported by the U.S. Department of Energy, Office of Science, under Contract No. DE-AC02-06CH11357.

References

1 W. Li, E. M. Erickson and A. Manthiram, High-nickel layered oxide cathodes for lithium-based automotive batteries, *Nat. Energy*, 2020, **5**, 26–34.
2 M. Li, J. Lu, Z. Chen and K. Amine, 30 years of lithium-ion batteries, *Adv. Mater.*, 2018, **30**, 1800561.
3 W. Li, S. Lee and A. Manthiram, High-Nickel NMA: A Cobalt-Free Alternative to NMC and NCA Cathodes for Lithium-Ion Batteries, *Adv. Mater.*, 2020, **32**, 2002718.
4 H. Liu, Z. Zhu, Q. Yan, S. Yu, X. He, Y. Chen, R. Zhang, L. Ma, T. Liu, M. Li, R. Lin, Y. Chen, Y. Li, X. Xing, Y. Choi, L. Gao, H. S. Cho, K. An, J. Feng, R. Kostecki, K. Amine, T. Wu, J. Lu, H. L. Xin, S. P. Ong and P. Liu, A disordered rock salt anode for fast-charging lithium-ion batteries, *Nature*, 2020, **585**, 63–67.
5 L. Zou, W. Zhao, Z. Liu, H. Jia, J. Zheng, G. Wang, Y. Yang, J.-G. Zhang and C. Wang, Revealing Cycling rate-dependent structure evolution in Ni-rich layered cathode materials, *ACS Energy Lett.*, 2018, **3**, 2433–2440.
6 E. Hu, X. Wang, X. Yu and X.-Q. Yang, Probing the Complexities of Structural Changes in Layered Oxide Cathode Materials for Li-Ion Batteries during Fast Charge-Discharge Cycling and Heating, *Acc. Chem. Res.*, 2018, **51**, 290–298.
7 S.-M. Bak, K.-W. Nam, W. Chang, X. Yu, E. Hu, S. Hwang, E. A. Stach, K.-B. Kim, K. Y. Chung and X.-Q. Yang, Correlating Structural Changes and Gas Evolution during the Thermal Decomposition of Charged $Li_xNi_{0.8}Co_{0.15}Al_{0.05}O_2$ Cathode Materials, *Chem. Mater.*, 2013, **25**, 337–351.
8 T. Liu, A. Dai, J. Lu, Y. Yuan, Y. Xiao, L. Yu, M. Li, J. Gim, L. Ma, J. Liu, C. Zhan, L. Li, J. Zheng, Y. Ren, T. Wu, R. Shahbazian-Yassar, J. Wen, F. Pan and K. Amine, Correlation between manganese dissolution and dynamic phase stability in spinel-based lithium-ion battery, *Nat. Commun.*, 2019, **10**, 4721.

9 L. Wang, A. Dai, W. Xu, S. Lee, W. Cha, R. Harder, T. Liu, Y. Ren, G. Yin, P. Zuo, J. Wang, J. Lu and J. Wang, Structural Distortion Induced by Manganese Activation in a Lithium-Rich Layered Cathode, *J. Am. Chem. Soc.*, 2020, **142**, 14966–14973.

10 Y. Xu, H. Wu, H. Jia, J. G. Zhang, W. Xu and C. Wang, Current Density Regulated Atomic to Nanoscale Process on Li Deposition and Solid Electrolyte Interphase Revealed by Cryogenic Transmission Electron Microscopy, *ACS Nano*, 2020, **14**, 8766–8775.

11 D. Qian, C. Ma, K. L. More, Y. S. Meng and M. Chi, Advanced analytical electron microscopy for lithium-ion batteries, *NPG Asia Mater.*, 2015, **7**, e193.

12 Q. Cheng, L. Wei, Z. Liu, N. Ni, Z. Sang, B. Zhu, W. Xu, M. Chen, Y. Miao, L. Q. Chen, W. Min and Y. Yang, Operando and three-dimensional visualization of anion depletion and lithium growth by stimulated Raman scattering microscopy, *Nat. Commun.*, 2018, **9**, 2942.

13 J. Zheng, T. Liu, Z. Hu, Y. Wei, X. Song, Y. Ren, W. Wang, M. Rao, Y. Lin, Z. Chen, J. Lu, C. Wang, K. Amine and F. Pan, Tuning of thermal stability in layered $Li(Ni_xMn_yCo_z)_2$, *J. Am. Chem. Soc.*, 2016, **138**, 13326–13334.

14 D. Liu, Z. Shadike, R. Lin, K. Qian, H. Li, K. Li, S. Wang, Q. Yu, M. Liu, S. Ganapathy, X. Qin, Q.-H. Yang, M. Wagemaker, F. Kang, X.-Q. Yang and B. Li, Review of Recent Development of In Situ/Operando Characterization Techniques for Lithium Battery Research, *Adv. Mater.*, 2019, **31**, 1806620.

15 A. M. Tripathi, W. N. Su and B. J. Hwang, In situ analytical techniques for battery interface analysis, *Chem. Soc. Rev.*, 2018, **47**, 736–851.

16 N. Taguchi, M. Kitta, H. Sakaebe, M. Kohyama and T. Akita, Lithium analysis using reflection EELS for lithium compounds, *J. Electron Spectrosc. Relat. Phenom.*, 2015, **203**, 40–44.

17 J. Cazaux, Secondary electron emission and charging mechanisms in Auger Electron Spectroscopy and related e-beam techniques, *J. Electron Spectrosc. Relat. Phenom.*, 2010, **176**, 58–79.

18 G. George, C. S. Edwards, J. I. Hayes, L. Yu, S. R. Ede, J. Wen and Z. Luo, A novel reversible fluorescent probe for the highly sensitive detection of nitro and peroxide organic explosives using electrospun $BaWO_4$ nanofibers, *J. Mater. Chem. C*, 2019, **7**, 14949–14961.

19 R. F. Egerton and M. Malac, EELS in the TEM, *J. Electron Spectrosc. Relat. Phenom.*, 2005, **143**, 43–50.

20 R. F. Egerton, Electron energy-loss spectroscopy in the TEM, *Rep. Prog. Phys.*, 2009, **72**, 016502.

21 P. E. Batson, N. Dellby and O. L. Krivanek, Sub-ångstrom resolution using aberration corrected electron optics, *Nature*, 2002, **418**, 617–620.

22 P. E. Batson, Simultaneous STEM imaging and electron energy-loss spectroscopy with atomic-column sensitivity, *Nature*, 1993, **366**, 727–728.

23 N. Jiang, B. Jiang, J. C. H. Spence, R. C. Yu, S. C. Li and C. Q. Jin, Anisotropic excitons in MgB_2 from orientation-dependent electron-energy-loss spectroscopy, *Phys. Rev. B: Condens. Matter Mater. Phys.*, 2002, **66**, 172502.

24 Y. Nomura, K. Yamamoto, M. Fujii, T. Hirayama, E. Igaki and K. Saitoh, Dynamic imaging of lithium in solid-state batteries by operando electron energy-loss spectroscopy with sparse coding, *Nat. Commun.*, 2020, **11**, 2824.

25 J. Kikkawa, S. Terada, A. Gunji, T. Nagai, K. Kurashima and K. Kimoto, Chemical States of Overcharged $LiCoO_2$ Particle Surfaces and Interiors Observed Using Electron Energy-Loss Spectroscopy, *J. Phys. Chem. C*, 2015, **119**, 15823–15830.

26 E. Hu, X. Yu, R. Lin, X. Bi, J. Lu, S. Bak, K.-W. Nam, H. L. Xin, C. Jaye, D. A. Fischer, K. Amine and X.-Q. Yang, Evolution of redox couples in Li-and Mn-rich cathode materials and mitigation of voltage fade by reducing oxygen release, *Nat. Energy*, 2018, **3**, 690–698.

27 K. Nakayama, R. Ishikawa, S. Kobayashi, N. Shibata and Y. Ikuhara, Dislocation and oxygen-release driven delithiation in Li_2MnO_3, *Nat. Commun.*, 2020, **11**, 4452.

28 Y. Liao, Pract. Electron Microsc. Database, http://www.glo balsino.com/EM.

29 R. Pal, A. K. Sikder, K. Saito, A. M. Funston and J. R. Bellare, Electron energy loss spectroscopy for polymers: a review, *Polym. Chem.*, 2017, **8**, 6927–6937.

30 M. Diociaiuti, Electron energy loss spectroscopy microanalysis and imaging in the transmission electron microscope: example of biological applications, *J. Electron Spectrosc. Relat. Phenom.*, 2005, **143**, 189–203.

31 V. J. Keast, A. J. Scott, R. Brydson, D. B. Williams and J. Bruley, Electron energy-loss near-edge structure-a tool for the investigation of electronic structure on the nanometre scale, *J. Microsc.*, 2001, **203**, 135–175.

32 M. Saitoh, X. Gao, T. Ogawa, Y. H. Ikuhara, S. Kobayashi, C. A. J. Fisher, A. Kuwabara and Y. Ikuhara, Systematic analysis of electron energy-loss near-edge structures in Li-ion battery materials, *Phys. Chem. Chem. Phys.*, 2018, **20**, 25052–25061.

33 F. Wang, J. Graetz, M. S. Moreno, C. Ma, L. Wu, V. Volkov and Y. Zhu, Chemical distribution and bonding of lithium in intercalated graphite: Identification with optimized electron energy loss spectroscopy, *ACS Nano*, 2011, **5**, 1190–1197.

34 F. Frati, M. O. J. Y. Hunault and F. M. F. de Groot, Oxygen K-edge X-ray absorption spectra, *Chem. Rev.*, 2020, **120**, 4056–4110.

35 J. Graetz, C. C. Ahn, H. Ouyang, P. Rez and B. Fultz, White lines and d-band occupancy for the 3d transition-metal oxides and lithium transition-metal oxides, *Phys. Rev. B: Condens. Matter Mater. Phys.*, 2004, **69**, 235103.

36 F. Lin, D. Nordlund, I. M. Markus, T.-C. Weng, H. L. Xin and M. M. Doeff, Profiling the nanoscale gradient in stoichiometric layered cathode particles for lithium-ion batteries, *Energy Environ. Sci.*, 2014, **7**, 3077–3085.

37 H. Kurata and C. Colliex, Electron-energy-loss core-edge structures in manganese oxides, *Phys. Rev. B: Condens. Matter Mater. Phys.*, 1993, **48**, 2102–2108.

38 B. Xiao, H. Liu, N. Chen, M. N. Banis, H. Yu, J. Liang, Q. Sun, T. K. Sham, R. Li, M. Cai, G. A. Botton and X. Sun, Size-Mediated Recurring Spinel Sub-nanodomains in Li- and Mn-Rich Layered Cathode Materials, *Angew. Chem., Int. Ed.*, 2020, **59**, 14313–14320.

39 C. Zhang, Y. Feng, B. Wei, C. Liang, L. Zhou, D. G. Ivey, P. Wang and W. Wei, Heteroepitaxial oxygen-buffering interface enables a highly stable cobalt-free Li-rich layered oxide cathode, *Nano Energy*, 2020, **75**, 104995.

40 A. K. Shukla, Q. M. Ramasse, C. Ophus, H. Duncan, F. Hage and G. Chen, Unravelling structural ambiguities in lithium- and manganese-rich transition metal oxides, *Nat. Commun.*, 2015, **6**, 8711.

41 Y. Sun, L. Wang, Y. Li, Y. Li, H. R. Lee, A. Pei, X. He and Y. Cui, Design of red phosphorus nanostructured electrode for fast-charging lithium-ion batteries with high energy density, *Joule*, 2019, **3**, 1080–1093.

42 H. Zhao, J. Chen, W. Wei, S. Ke, X. Zeng, D. Chen and P. Lin, Synthesis of Ni@NiSn Composite with High Lithium-Ion Diffusion Coefficient for Fast-Charging Lithium-Ion Batteries, *Glob. Chall.*, 2020, **4**, 1900073.

43 W. Zhang, D.-H. Seo, T. Chen, L. Wu, M. Topsakal, Y. Zhu, D. Lu, G. Ceder and F. Wang, Kinetic pathways of ionic transport in fast-charging lithium titanate, *Science*, 2020, **367**, 1030–1034.

44 G. Qian, Y. Zhang, L. Li, R. Zhang, J. Xu, Z. Cheng, S. Xie, H. Wang, Q. Rao, Y. He, Y. Shen, L. Chen, M. Tang and Z.-F. Ma, Single-crystal nickel-rich layered-oxide battery cathode materials: synthesis, electrochemistry, and intragranular fracture, *Energy Storage Mater.*, 2020, **27**, 140–149.

45 T. Wu, X. Liu, X. Zhang, Y. Lu, B. Wang, Q. Deng, Y. Yang, E. Wang, Z. Lyu, Y. Li, Y. Wang, Y. Lyu, C. He, Y. Ren, G. Xu, X. Sun, K. Amine and H. Yu, Full Concentration Gradient-Tailored Li-Rich Layered Oxides for High-Energy Lithium-Ion Batteries, *Adv. Mater.*, 2021, **33**, 2001358.

46 Y. Koyama, T. Mizoguchi, H. Ikeno and I. Tanaka, Electronic structure of lithium nickel oxides by electron energy loss spectroscopy, *J. Phys. Chem. B*, 2005, **109**, 10749–10755.

47 C. Xu, K. Marker, J. Lee, A. Mahadevegowda, P. J. Reeves, S. J. Day, M. F. Groh, S. P. Emge, C. Ducati, B. Layla Mehdi, C. C. Tang and C. P. Grey, Bulk fatigue induced by surface reconstruction in layered Ni-rich cathodes for Li-ion batteries, *Nat. Mater.*, 2021, **20**, 84–92.

48 S. Li, Z. Jiang, J. Han, Z. Xu, C. Wang, H. Huang, C. Yu, S. J. Lee, P. Pianetta, H. Ohldag, J. Qiu, J. S. Lee, F. Lin, K. Zhao and Y. Liu, Mutual modulation between surface chemistry and bulk microstructure within secondary particles of nickel-rich layered oxides, *Nat. Commun.*, 2020, **11**, 4433.

49 X. Li, Z. Ren, M. Norouzi Banis, S. Deng, Y. Zhao, Q. Sun, C. Wang, X. Yang, W. Li, J. Liang, X. Li, Y. Sun, K. Adair, R. Li, Y. Hu, T.-K. Sham, H. Huang, L. Zhang, S. Lu, J. Luo and X. Sun, Unravelling the chemistry and microstructure evolution of a cathodic interface in sulfide-based all-solid-state Li-ion batteries, *ACS Energy Lett.*, 2019, **4**, 2480–2488.

50 M. Zhang, Z. Li, L. Yu, D. Kong, Y. Li, B. Cao, W. Zhao, J. Wen and F. Pan, Enhanced long-term cyclability in Li-Rich layered oxides by electrochemically constructing a $Li_xTM_{3-x}O_4$-type spinel shell, *Nano Energy*, 2020, **77**, 105188.

51 O. L. Krivanek, N. Dellby, J. A. Hachtel, J. C. Idrobo, M. T. Hotz, B. Plotkin-Swing, N. J. Bacon, A. L. Bleloch, G. J. Corbin, M. V. Hoffman, C. E. Meyer and T. C. Lovejoy, Progress in ultrahigh energy resolution EELS, *Ultramicroscopy*, 2019, **203**, 60–67.

52 J. Gázquez, G. Sánchez-Santolino, N. Biškup, M. A. Roldán, M. Cabero, S. J. Pennycook and M. Varela, Applications of STEM-EELS to complex oxides, *Mater. Sci. Semicond. Process.*, 2017, **65**, 49–63.

53 A. Gloter, V. Badjeck, L. Bocher, N. Brun, K. March, M. Marinova, M. Tencé, M. Walls, A. Zobelli, O. Stéphan and C. Colliex, Atomically resolved mapping of EELS fine structures, *Mater. Sci. Semicond. Process.*, 2017, **65**, 2–17.

54 T. Weigel, F. Schipper, E. M. Erickson, F. A. Susai, B. Markovsky and D. Aurbach, Structural and Electrochemical Aspects of $LiNi_{0.8}Co_{0.1}Mn_{0.1}O_2$ Cathode Materials Doped by Various Cations, *ACS Energy Lett.*, 2019, **4**, 508–516.

55 H. Li, P. Zhou, F. Liu, H. Li, F. Cheng and J. Chen, Stabilizing nickel-rich layered oxide cathodes by magnesium doping for rechargeable lithium-ion batteries, *Chem. Sci.*, 2019, **10**, 1374–1379.

56 Y. Shi, K. Kim, Y. Xing, A. Millonig, B. Kim, L. Wang, E. Lee, C. Harrison, T. Yu, D. C. Johnson, A. L. Lipson, J. L. Durham, D. Liu, T. T. Fister, L. Yu and J. Wen, Facile and scalable dry surface doping technique to enhance the electrochemical performance of $LiNi_{0.64}Mn_{0.2}Co_{0.16}O_2$ cathode materials, *J. Mater. Chem. A*, 2020, **8**, 19866–19872.

57 R. S. Negi, S. P. Culver, A. Mazilkin, T. Brezesinski and M. T. Elm, Enhancing the Electrochemical Performance of $LiNi_{0.70}Co_{0.15}Mn_{0.15}O_2$ Cathodes Using a Practical Solution-Based Al_2O_3 Coating, *ACS Appl. Mater. Interfaces*, 2020, **12**, 31392–31400.

58 J. Zheng, M. Gu, J. Xiao, B. J. Polzin, P. Yan, X. Chen, C. Wang and J.-G. Zhang, Functioning Mechanism of AlF_3 Coating on the Li- and Mn-Rich Cathode Materials, *Chem. Mater.*, 2014, **26**, 6320–6327.

59 F. C. Castro and V. P. Dravid, Characterization of Lithium Ion Battery Materials with Valence Electron Energy-Loss Spectroscopy, *Microsc. Microanal.*, 2018, **24**, 214–220.

60 X. Yan, C. Liu, C. A. Gadre, L. Gu, T. Aoki, T. C. Lovejoy, N. Dellby, O. L. Krivanek, D. G. Schlom, R. Wu and X. Pan, Single-defect phonons imaged by electron microscopy, *Nature*, 2021, **589**, 65–69.